Althaus

AIRFOILS WITH A NEW HINGE FOR AILERONS AND FLAPS

by

D. Althaus and R. Eppler
Universität Stuttgart

Introduction

Every sailplane designer knows that the air blowing through the slot of an aileron or flap causes considerable parasitic drag. For example, the well-known RJ5 had its best performance with fixed flaps and a filled slot [1]. For the same reason modern sailplanes have less aileron span than earlier types.

A certain improvement can be made by sticking a tape over the slots, but this tape has to form corners and wrinkles while moving the aileron or flap, and one can still find considerable parasitic drag.

The best aerodynamic solution presented so far has been the use of an elastic upper surface, for example in the well-known HKS sailplanes developed in the early fifties by Haase, Kensche and Schmetz. However, as a consequence of this, they had very high stick forces. The elastic slot cover had to carry all the forces between wing and flap and had to be rather strong.

In this paper a new design of a hinge is presented which allows for a very thin elastic cover for the slot between wing and flaps or ailerons, thus combining the advantages of the low stick forces of normal sailplanes with the favorable aerodynamics of the HKS sailplanes. Moreover, since the best solution for automatic correspondence between flap position and airspeed is a simple mechanical connection of the elevator and flap, causing additional elevator stick forces, we present a new airfoil having a good drag polar with minimum flap deflection.

The hinge mechanism

A particular ideal motion of the aileron or flap is sketched in Fig. 1 for the special case of an airfoil with a flat upper surface. For the case without deflection we imagine that the slot of length a is covered by a flat, thin elastic sheet. With deflection, this cover is assumed to be a circular arc of the same length a. Obviously it is not possible to approximate this ideal motion by a single hinge, as different

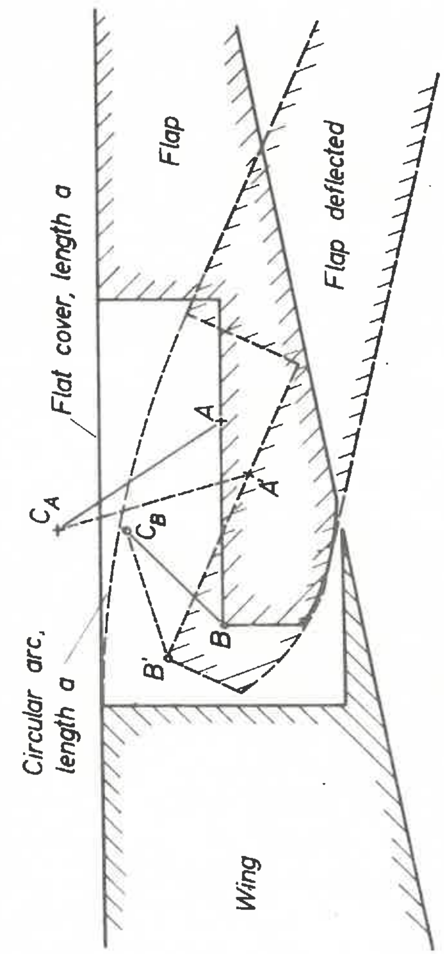

Figure 1. Ideal motion of a flap.

points of the flap A, A' or B, B' have different centers of motion C_A or C_B, but a very good approximation of the ideal motion is possible by connecting two different points of the flap, by single bars, with their centers of motion. Of course, it is no problem to find for any point of the flap the center of motion for the prescribed ideal motion of the flap. The only problem is to find two points in the flap so that the two centers of motion have enough distance for arranging the bearings and the bars and so that the entire hinge has as few parts as possible above the upper side of the airfoil. The hinges can be covered by a little rubber hat, and the parts between the hinges by a thin elastic sheet, which forms approximately a circular arc during the deflection of the flap. In Fig. 2 a typical solution in three flap positions is shown.

In the case of an airfoil with a cambered upper surface we have the flat slot cover not as it is sketched in Figures 1 and 2 for the undeflected flap, but with some small flap deflection.

Obviously the double hinge can be produced for a certain length a of the slot cover. Thus the designer may use a prefabricated double hinge instead of a (normally also prefabricated) single hinge, and has to prepare a slot of given width a.

A kinematic model and a production prototype of the double hinge have been constructed.

The airfoil

As mentioned previously, a mechanical connection between elevator and flap is a simple solution for automatic optimal flap position. Such a connection causes additional elevator stick forces, although there exists a certain effect of the airloads on the flap, which allows one to decrease these forces considerably by using a spring. Thus it is desirable to have maximum flap effect with only a small flap chord and deflection. Even without flap-elevator connection, one can show, and see in many experimental data that really good L/D ratios are always reached with a small flap deflection only.

The fundamental problem of flapped airfoils is sketched in Fig. 3. A conventional laminar airfoil at an angle-of-attack near the upper edge of the laminar bucket has a more-or-less constant velocity over the laminar section of the upper surface. Flap deflection down causes a suction peak near the flap hinge. Additional angle-of-attack causes a suction peak near the leading edge. Thus the velocity distribution becomes a very unfavorable shape for laminar effects. While in the rear part of the airfoil the pressure gradient is still favorable, no laminar flow exists due to the adverse pressure gradient near the leading edge. The adverse pressure

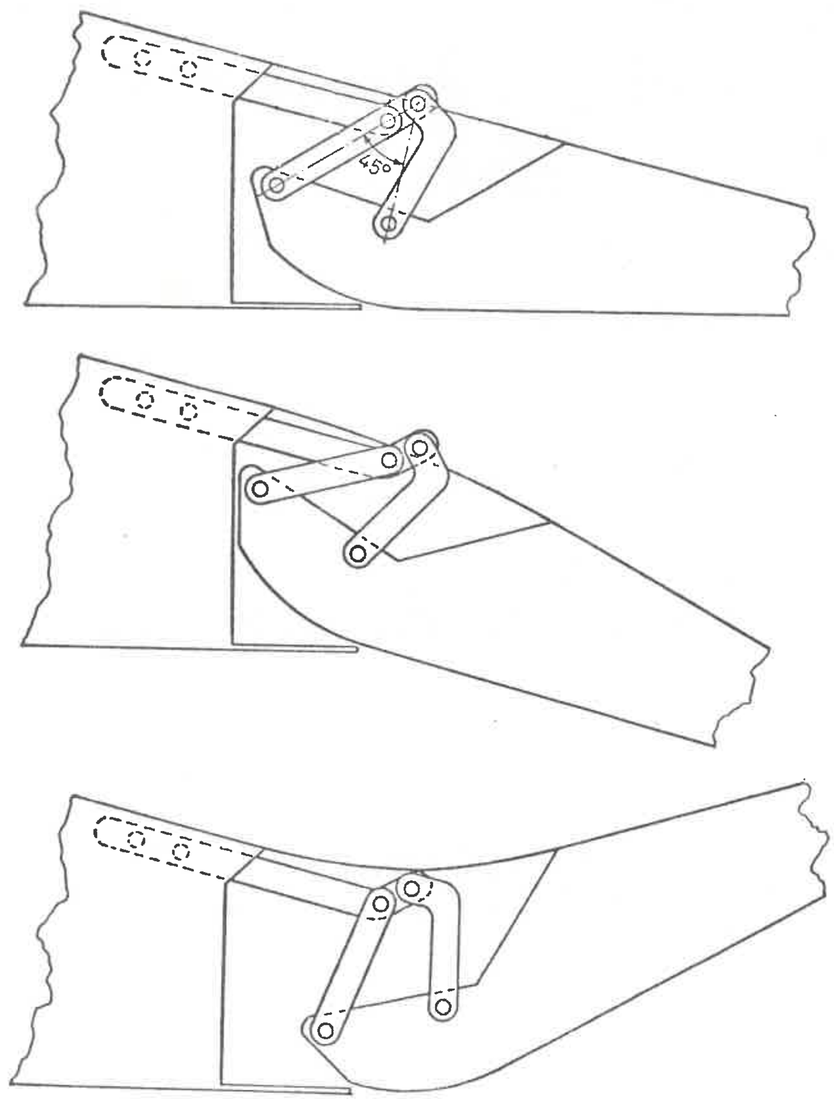

Figure 2. Double-hinge flap in 3 positions.

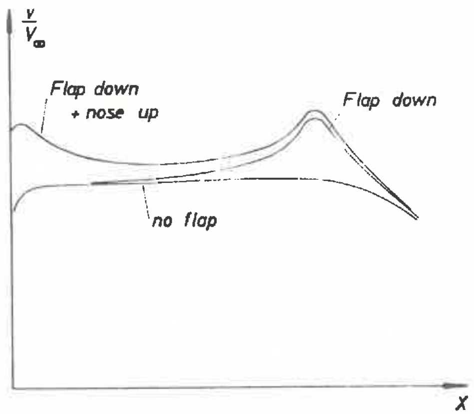

Figure 3. Influence of flaps on the velocity distribution of a laminar airfoil, upper surface.

gradient near the trailing edge causes separation of the turbulent boundary layer arriving there with considerable thickness.

Prevention of this cow-belly like velocity distribution promises improvements. However, until now airfoil shape computation starting from a given pressure distribution [2,3] has only been possible for one airfoil configuration. Now the problem is different. We need for the flapped airfoil a given pressure distribution on the upper surface, while for the unflapped airfoil the lower surface is most important, since it determines the lower end of the laminar bucket.

To solve this problem, the usual method for direct computation of an airfoil shape from the pressure distribution [2,3] has been extended. The fundamental idea was to give, in some region, fixed parameters for the properties of the pressure distribution, while the parameters in other parts of the airfoil are used for a least-squares fit to a given shape.

It is not possible to present the details of this method here. The method developed uses an iteration process of the following kind:

1. Firstly, an airfoil $A^{(o)}$ for the high-speed case is computed, which has low drag at low C_L and high Reynolds number. We assumed about 75% laminar flow on the lower surface and 55% on the upper surface. As an example, for a velocity distribution meeting these conditions for an angle-of-attack of 1° or a C_L of 0.11 we can use Fig. 4. The adverse pressure gradient, or the decrease of velocity in the region of the trailing edge is chosen such that the airfoil has a thickness of about 15%. On both sides, at $Re = 3 \cdot 10^6$ only short destabilization areas are needed to prevent laminar separation bubbles. The over-all pressure rise on the upper surface is less than it would be without turbulent separation, thus a certain reserve for the suction peak of the flap exists. It should be noticed that the velocity distribution of the lower surface shows a little adverse pressure gradient near the leading edge and a very little favorable pressure gradient behind x = 50%. This is the optimal distribution near transition. The methods giving this result are described in [4]. For the upper surface it is required only that transition lies behind 55% chord. The details of the pressure distribution before this point are free for airfoil A^o and are chosen arbitrarily.
2. Secondly, an airfoil $B^{(o)}$ for the high-lift case and smaller Re is computed, which has given properties of the pressure distribution over the first 50% of the upper side and approximates airfoil $A^{(o)}$ for the

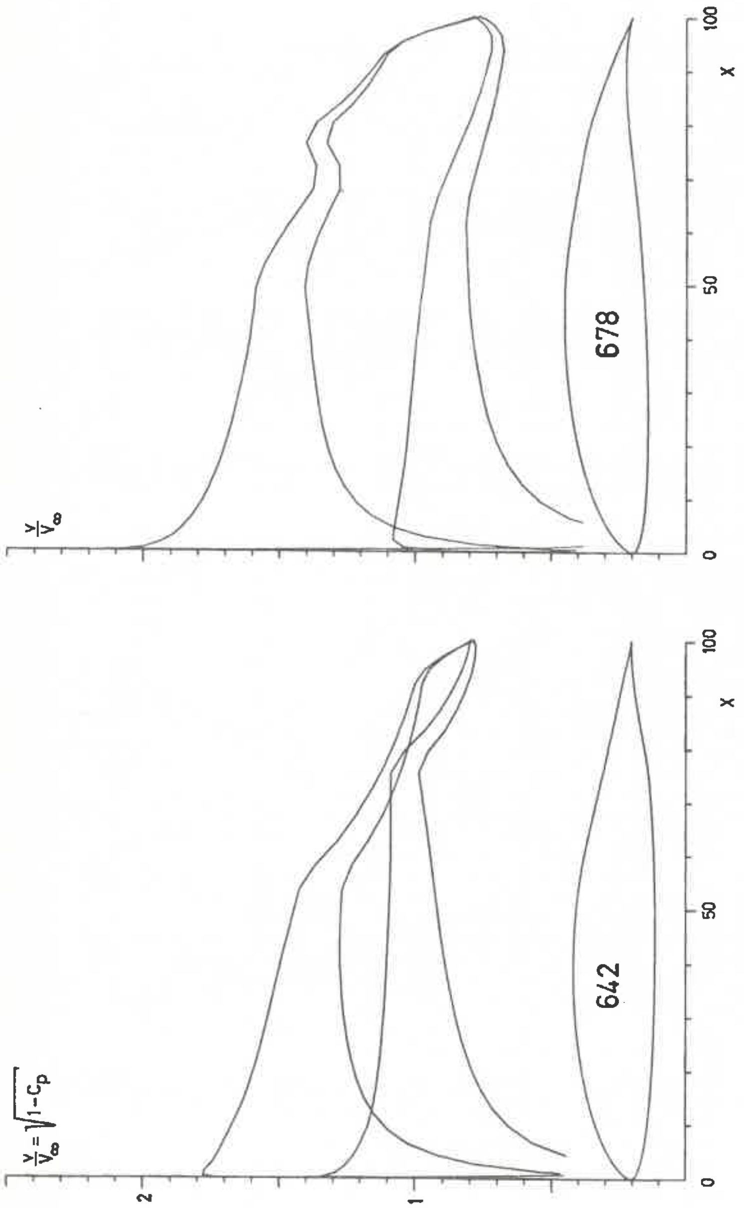

Figure 4. Airfoils 642 and 678 and their theoretical velocity distributions

upper side between 50% and 70% and for the lower side between 0 and 70%.

3. Airfoil $A^{(i+1)}$ keeps the areas of given pressure distributions of airfoil $A^{(o)}$ and approximates airfoil $B^{(i)}$ in the area originally having an arbitrary pressure distribution. This approximation also influences somewhat the shape of the airfoil in the part in which the pressure distribution does not change.
4. Airfoil $B^{(i+1)}$ keeps the area of given pressure distribution of airfoil $B^{(o)}$ and approximates airfoil $A^{(i+1)}$ in the same areas where airfoil $B^{(o)}$ approximated airfoil $A^{(o)}$. This approximation again influences the shape of the airfoil very slightly in the part with unchanging pressure distribution.
5. If the difference between airfoil $B^{(i+1)}$ and airfoil $B^{(i)}$ is small enough, the iteration process is terminated. Otherwise it continues with step 3.

The approximation process used in each step of the iteration process is not very fully automated and still needs some effort. However, the convergence of the iteration process is very rapid, and only 1 or 2 iterations are usually needed.

A typical result is shown in Fig. 4. The two airfoils coincide over the first 70% of the chord, and can be considered as unflapped (No. 642) and flapped (No. 678) airfoils, having for the front portions, as exactly as possible, the desired pressure distribution features. Airfoil 678 has the typical suction peak of a flap just behind the end of the portion over which it coincides with airfoil 642.

On both sides, when the flap is deflected down, longer destabilization areas develop. These are necessary, at lower Reynolds numbers, to prevent laminar separation bubbles. A wind-tunnel model of airfoil 642 has been built, with a double hinge flap at 75% chord. The 10° flap-down position approximated airfoil 678 very well. The measurements are shown in Figs. 5 and 6.

The results are disappointing in two respects. The minimum drag of 642 is higher than expected from the boundary layer computations. This is probably due to an inexact fit of the flap at the lower surface. The slope of the C_D-polar for $Re = 3 \cdot 10^6$ agreed very well with the theoretical results, however.

Also, the maximum lift measured was not as high as the theoretical value. We therefore looked for laminar separation bubbles, but found none. The turbulent separation was found to occur a little too early. This is probably due to a too-long instability area. The turbulent boundary layers are already too thick when reaching the adverse pressure gradient

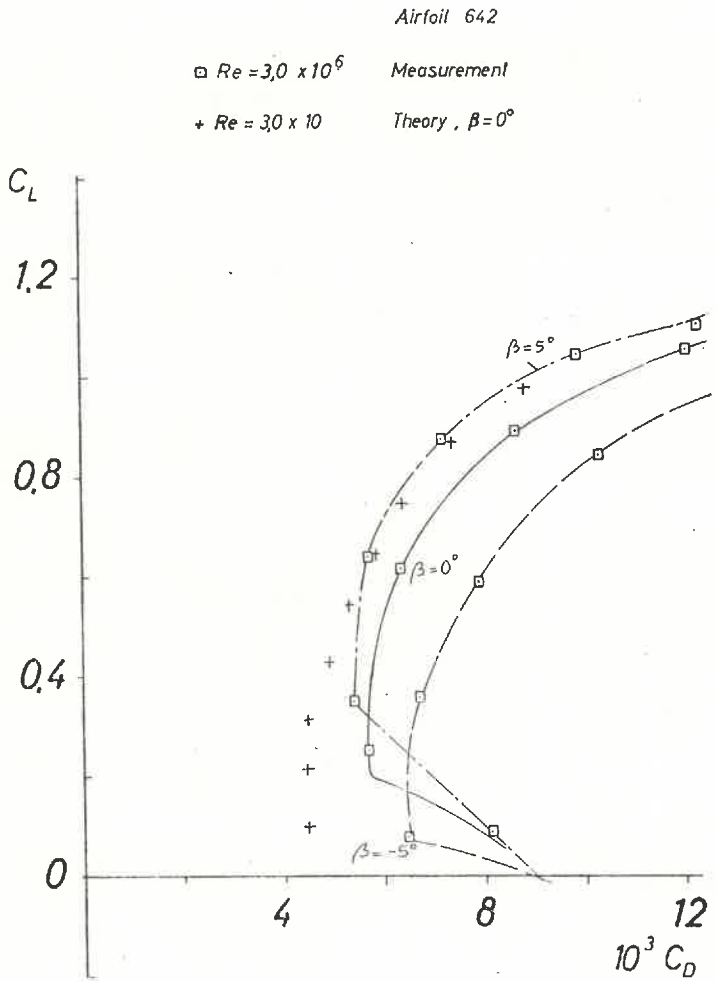

Figure 5. Theoretical and experimental drag polar of airfoil 642.

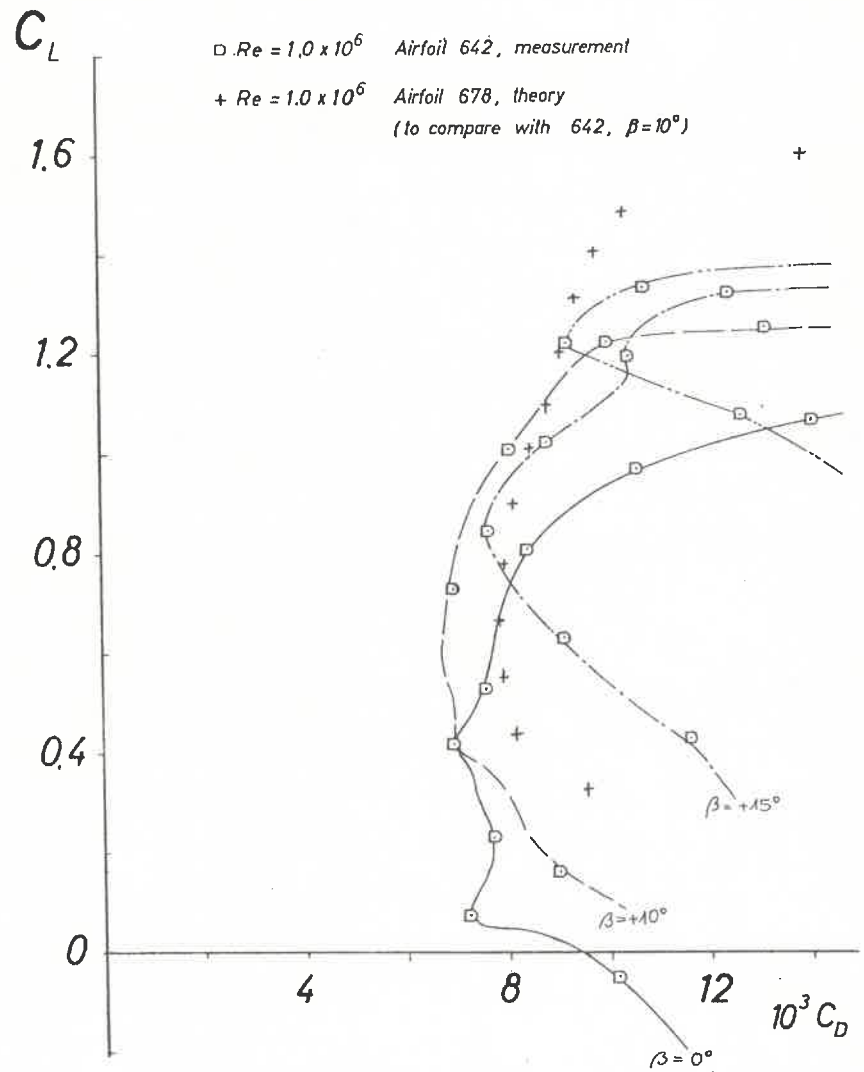

Figure 6. Theoretical drag polar of airfoil 678, experimental drag polar of flapped airfoil 642.

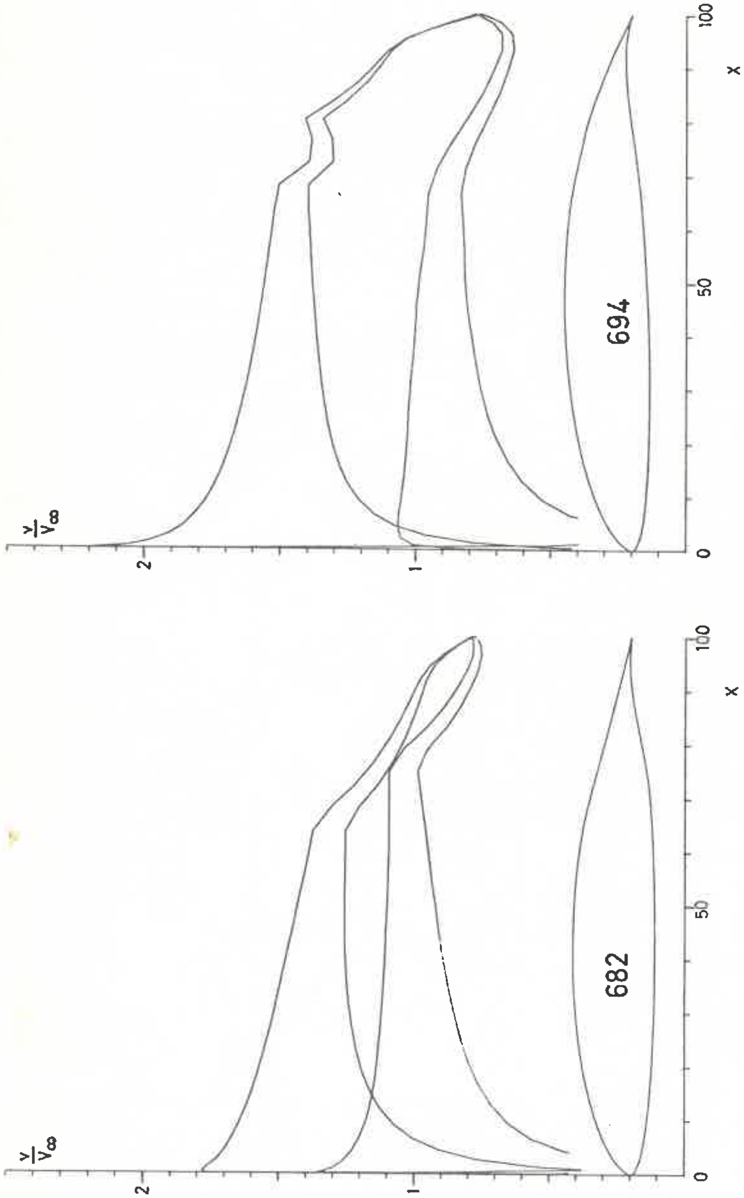

Figure 7. Airfoils 682 and 694 and their theoretical velocity distributions

Table 1

PROFIL 642 X	Y	PROFIL 678 X	Y	PROFIL 682 X	Y	PROFIL 694 X	Y
100.000	0.000	100.000	0.000	100.000	0.000	100.000	0.000
99.624	0.059	99.642	0.136	99.623	0.065	99.640	0.142
98.541	0.268	98.640	0.567	98.534	0.288	98.632	0.588
96.849	0.651	97.130	1.277	96.823	0.697	97.110	1.325
94.630	1.170	95.207	2.172	94.572	1.265	95.172	2.263
91.917	1.770	92.880	3.159	91.825	1.953	92.835	3.313
88.712	2.441	90.140	4.216	88.608	2.751	90.100	4.450
85.055	3.206	87.031	5.349	84.978	3.671	87.023	5.674
81.019	4.071	83.638	6.529	81.020	4.707	83.699	6.943
76.683	5.025	80.043	7.663	76.825	5.828	80.202	8.112
72.129	6.048	76.219	8.613	72.490	6.990	76.399	9.069
67.445	7.103	72.033	9.395	68.113	8.095	72.246	9.999
62.717	8.143	67.527	10.178	63.704	9.002	67.996	10.909
58.027	9.082	62.908	10.983	59.178	9.665	63.668	11.587
53.386	9.807	58.280	11.688	54.523	10.146	59.165	12.054
48.735	10.285	53.659	12.219	49.799	10.473	54.541	12.360
44.073	10.561	49.047	12.528	45.059	10.649	49.844	12.506
39.447	10.660	44.427	12.613	40.352	10.676	45.125	12.502
34.904	10.588	39.817	12.514	35.726	10.555	40.431	12.347
30.483	10.355	35.275	12.256	31.224	10.288	35.810	12.049
26.227	9.972	30.849	11.848	26.889	9.884	31.310	11.612
22.178	9.451	26.585	11.298	22.764	9.350	26.975	11.043
18.377	8.803	22.526	10.617	18.889	8.696	22.848	10.352
14.860	8.041	18.710	9.816	15.299	7.931	18.968	9.540
11.660	7.180	15.174	8.908	12.027	7.071	15.373	8.646
8.807	6.233	11.950	7.910	9.103	6.133	12.095	7.658
6.326	5.218	9.069	6.838	6.554	5.132	9.166	6.603
4.231	4.156	6.554	5.711	4.397	4.091	6.608	5.499
2.536	3.080	4.425	4.553	2.649	3.038	4.445	4.369
1.259	2.025	2.695	3.392	1.328	2.006	2.692	3.239
0.414	1.027	1.379	2.261	0.446	1.031	1.365	2.141
0.012	0.147	0.488	1.200	0.017	0.171	0.469	1.113
0.176	-0.536	0.032	0.269	0.166	-0.501	0.025	0.218
0.980	-1.102	0.117	-0.437	0.961	-1.071	0.146	-0.466
2.366	-1.649	0.827	-0.991	2.333	-1.627	0.908	-1.022
4.292	-2.152	2.123	-1.491	4.246	-2.143	2.249	-1.539
6.734	-2.602	3.973	-1.914	6.674	-2.611	4.135	-1.989
9.669	-2.998	6.351	-2.264	9.595	-3.029	6.544	-2.367
13.064	-3.346	9.229	-2.538	12.974	-3.401	9.455	-2.673
16.874	-3.648	12.574	-2.737	16.768	-3.728	12.854	-2.915
21.053	-3.902	16.352	-2.865	20.929	-4.008	16.640	-3.096
25.551	-4.108	20.517	-2.929	25.409	-4.239	20.823	-3.222
30.313	-4.265	25.017	-2.931	30.152	-4.420	25.325	-3.289
35.285	-4.370	29.798	-2.869	35.105	-4.549	30.099	-3.286
40.408	-4.425	34.810	-2.744	40.207	-4.623	35.099	-3.217
45.622	-4.426	39.992	-2.560	45.401	-4.641	40.268	-3.093
50.865	-4.374	45.287	-2.311	50.625	-4.602	45.534	-2.912
56.078	-4.266	50.649	-2.000	55.817	-4.502	50.840	-2.661
61.195	-4.103	56.014	-1.644	60.915	-4.342	56.148	-2.343
66.152	-3.877	61.306	-1.230	65.853	-4.112	61.389	-1.982
70.885	-3.576	66.499	-0.723	70.567	-3.800	66.472	-1.556
75.531	-3.154	71.611	-0.147	74.994	-3.356	71.304	-1.000
79.522	-2.539	76.619	0.410	79.167	-2.699	76.177	-0.334
83.562	-1.798	81.446	0.859	83.209	-1.895	80.862	0.336
87.424	-1.108	85.979	1.129	87.103	-1.132	85.382	0.875
90.970	-0.568	90.078	1.192	90.715	-0.531	89.596	1.161
94.070	-0.207	93.612	1.050	93.901	-0.137	93.310	1.141
96.604	-0.020	96.441	0.741	96.520	0.045	96.309	0.845
98.475	0.034	98.449	0.377	98.447	0.069	98.414	0.432
99.617	0.017	99.619	0.101	99.612	0.026	99.615	0.114
100.000	0.000	100.000	0.000	100.000	0.000	100.000	0.000
$C_{Mo}=0.0551$	$\beta=2.80°$	$C_{Mo}=0.2062$	$\beta=7.76°$	$C_{Mo}=0.0701$	$\beta=3.25°$	$C_{Mo}=0.2115$	$\beta=7.85°$

behind the flap hinge. Wortmann [5] has remarked that in such a situation the boundary layer theory may sometimes fail.

An improvement should be possible by taking a longer area of laminar boundary layer on the upper surface, as calculated for the airfoil combination 682/694. The shapes and velocity distributions are shown in Fig. 7. The wind-tunnel experiments have been prepared but still await execution.

The coordinates, angles of zero lift and moment coefficients of all the airfoils discussed are given in Table 1.

References

1. Raspet, A.; Systematic Improvements of the Drag Polar of the Sailplane RJ5, Soaring 1951, Nr. 5.

2. Eppler, R.; Direkte Berechnung von Tragflügelprofilen aus der Druckverteilung. Ing.-Arch. 25 (1957), S. 32-57.

3. Eppler, R.; Über die Entwicklung moderner Tragflügelprofile. De Ingenieur 77 (1965), S. L17-L22.

4. Eppler, R.; Laminarprofile für Reynolds-Zahlen grösser als $4 \cdot 10^6$. Ing.-Arch. 38 (1969), S. 232-240.

5. Wortmann, F.X.; A Critical Review on the Physical Aspects of Airfoil Design at Low Mach Numbers, Proceedings of the First International Symposium on the Technology and Science of Motorless Flight, M.I.T., Cambridge, Mass., October 1972.